APL Materials ARTICLE scitation.org/journal/apm

Controlling thermal conductance using three-dimensional phononic crystals

Cite as: APL Mater. 9, 081108 (2021); doi: 10.1063/5.0057385
Submitted: 20 May 2021 • Accepted: 23 July 2021 •
Published Online: 13 August 2021

Samuli Heiskanen, Tuomas A. Puurtinen, and Ilari J. Maasilta[a)]

AFFILIATIONS

Department of Physics, Nanoscience Center, University of Jyvaskyla, P.O. Box 35, FIN-40014 Jyväskylä, Finland

Note: This paper is part of the Special Topic on Phononic Crystals at Various Frequencies.
[a)]**Author to whom correspondence should be addressed:** maasilta@jyu.fi

ABSTRACT

Controlling thermal transport at the nanoscale is vital for many applications. Previously, it has been shown that this control can be achieved with periodically nanostructured two-dimensional phononic crystals for the case of suspended devices. Here, we show that thermal conductance can also be controlled with three-dimensional phononic crystals, allowing the engineering of the thermal contact of more varied devices without the need for suspension in the future. We show the experimental results obtained at sub-Kelvin temperatures for two different period three-dimensional crystals and for a bulk control structure. The results show that the conductance can be enhanced with the phononic crystal structures in our geometry. This result cannot be fully explained by the simplest theory taking into account the coherent modification of the phonon band structure, calculated by finite element method simulations.

I. INTRODUCTION

Phononic crystals (PnCs) are periodic structures that are the elastic analogs of the more widely known photonic crystals.[1] Instead of a periodic dielectric constant, they have a periodic density and elasticity. This means that they can be used to manipulate how vibrational energy (sound and/or heat) flows through a material (for a recent review, see Ref. 2). The flow of energy can be altered due to changes introduced into the material's phononic band structure or scattering efficiency. PnCs can even produce full bandgaps at specific frequencies due to Bragg interference[3,4] or local resonances.[5–7] Due to the ease of fabrication, early experiments focused on macroscopic structures with periods in the millimeter-scale.[8] Structures like this are typically applied in acoustic filtering, focusing, or wave-guiding[5,8–10] because their dominant frequency is in the range of sonic or ultrasonic waves. Advancements in fabrication methods, such as colloidal crystallization and interference lithography, allowed the fabrication of structures with micro- and nano-scale periods, which have hypersonic dominant frequencies.[7,11,12] Such structures can be applied, for example, in RF communication devices[13] and also in thermal transport, as hypersonic ~ 10 GHz frequencies are dominant for thermal phonons at low temperatures.[14]

However, not a lot of work has been done on the thermal properties of micro- and nano-scale PnC structures (for reviews, see Refs. 6 and 15). This is especially the case with low temperature studies where the coherent modification of the band structure is still operational and not destroyed by disorder.[16,17] There have been low temperature experimental studies on 2D holey PnC structures fabricated into a thin SiN membrane,[14,18] but no such studies have been done on 3D PnCs before. In the non-coherent regime at around room temperature, a couple of thermal transport studies have been performed using nanoscale 3D PnCs fabricated with colloidal crystallization techniques.[19,20]

The control of thermal transport has become vital for several applications. There is a need to improve the heat dissipation out of semiconductor devices, and better thermal isolation is needed, for example, in ultrasensitive bolometric radiation detectors.[21] Similarly, there are plans to use PnC structures to control thermal transport in quantum bits.[22] Previously, this kind of control was achieved by introducing scattering centers, such as nanoparticles or impurities, into the material.[23–25] However, it has been shown that thermal transport can also be controlled with periodic PnC structures.[19,20,26–28] It has been theoretically and experimentally demonstrated[14] that at low temperatures, PnCs alter the thermal conductance of the material by the coherent modification of its

phononic band structure. This was shown for 2D crystals, but similar ideas can be pursued also for 3D crystals, as discussed in this study. Considering different applications, the benefit of 3D crystals is that they make the isolation of any type of device possible, while 2D crystals only allow the isolation using more fragile suspended structures.

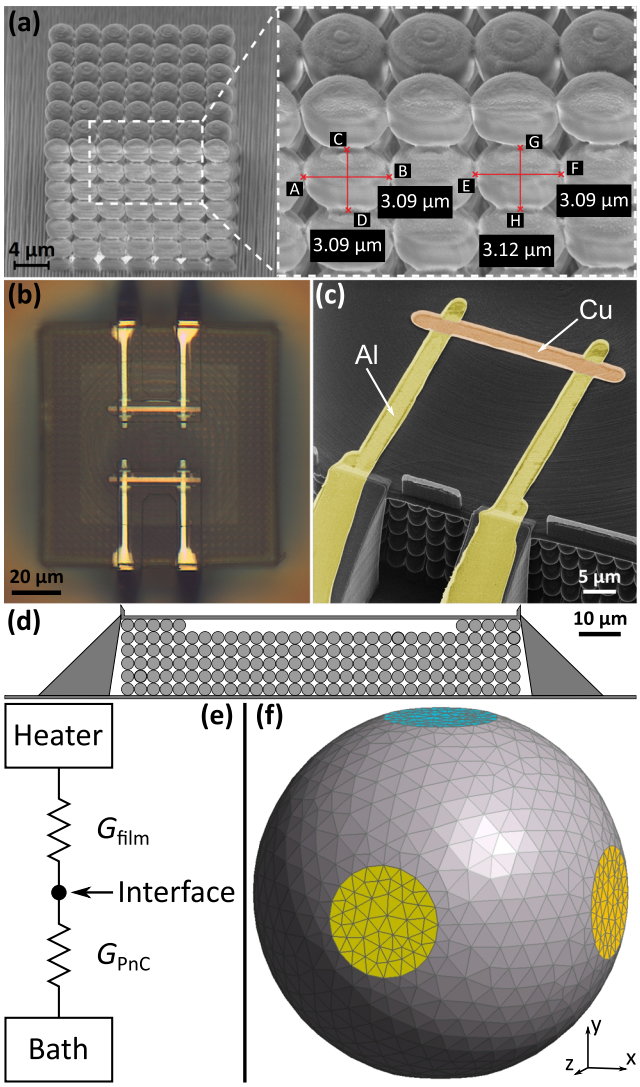

FIG. 1. (a) A SEM image of the 3.1 μm PnC lattice with half spheres at the front face. The image was taken at an angle of 45°, so the half spheres appear to be elliptical. (b) An optical microscopy image of the finished structure from the top, including the heater and thermometer devices. (c) A false color helium ion micrograph of a finished SINIS junction pair on a PnC structure (yellow = Al and orange = Cu). The linewidth is around 3 μm on the platform, giving a junction area of 9 μm^2. (d) A schematic cross-section of the 3.1 μm PnC structure. (e) The thermal model used in the analysis. (f) The FEM mesh used in the PnC simulations. For clarity, only the surface of the unit cell is shown, and the mesh extends into the sphere volume. Contact areas between neighboring spheres are shown in yellow and blue.

As already mentioned above, it has been shown that self-assembly can be used for the fabrication of 3D PnCs by colloidal crystallization of mono-disperse spherical particles.[7,12,19,20,29–31] However, there is no easy way to integrate sophisticated measurement devices and circuitry with such crystals. There have been efforts to allow the fabrication of metallic wires on these crystals by hardening the spheres with an electron beam,[32] but issues still exist with the continuity of the wiring due to the cracking of the crystals and separation at the substrate interface during drying.

In this study, in contrast, 3D laser lithography is used for crystal fabrication. The measurement devices and wiring were fabricated using a method developed for general device fabrication on high topographies, which utilizes the same 3D lithography tool but in combination with lift-off.[33] The 3D lithography technique is based on two-photon absorption, which allows the fabrication of arbitrary 3D structures from negative resists,[34–36] with a resolution of about 200 nm. 3D laser lithography was recently used to make an advanced 3D PnC structure for the first time,[10] but in that study, the focus was on controlling ultrasound at MHz frequencies, which allowed much larger periodicities (~300 μm), whereas here we need to push the resolution limits to influence GHz frequency phonons. Other additive manufacturing techniques (3D printing) have also been used to study macroscale 3D PnCs at sonic frequencies.[37–41] Compared to colloidal crystallization, 3D lithography is the more versatile fabrication method, which also means that devices can be integrated more easily with the 3D structures. However, we are limited to micrometer-scale crystal periods due to the resolution limit of the technique.

Here, we show with measurements and theoretical simulations that 3D PnCs fabricated by 3D lithography can be used to control sub-Kelvin thermal transport by orders of magnitude. We fabricated 3D simple cubic lattices of spheres to obtain 3D PnCs that support a heated platform (Fig. 1). This geometry was chosen for simplicity of fabrication and modeling. Crystals with two different lattice constants were fabricated: one with a smaller lattice constant (3.1 μm), which still resulted in a good spherical shape, and another larger period one (5.0 μm), which could still be feasibly simulated using the finite element method (FEM). The contact area between the spheres was minimized within the resolution limits of the 3D lithography tool (diameter: ~ 1 μm for the smaller PnC). The size of the crystal and the filling factor of the lattice were the same for both PnCs, which means that classical diffusive bulk scattering would give identical thermal conductances for both structures. However, our experiments show an order of magnitude difference between the two. Coherent simulations indeed predict a difference and also a strong suppression compared to a bulk structure. Unexpectedly, for both structures, the conductance was enhanced compared to a bulk control device. The reason for this is not clear yet and requires further study.

II. FABRICATION METHODS

The PnC structures are fabricated with a Nanoscribe Photonic Professional 3D lithography system. The 3D exposure was done with the dip-in mode where an objective is brought in direct contact with a liquid resist. For the structures in this study, we used the Ip-Dip resist from Nanoscribe GmbH. After the pattern of the structure is exposed into the liquid resist, development is done with propylene

glycol methyl ether acetate (PGMEA) for 20 min and the sample is rinsed with isopropanol (IPA). Then, a post-print UV curing is done for the samples,[42] which strengthens the structure and minimizes the shrinkage of the resist, as follows: Keeping the sample in solution, it is directly transferred to an IPA bath containing 0.5 wt. % 2,2-dimethoxy-2-phenylacetophenone (DMPA) and then exposed to a 366 nm UV light for 20 min. The added DMPA acts as a photoinitiator, and thus, this process increases cross-linking in the structure. Then, the sample is rinsed again with IPA and dried with N_2 gas. The PnC structures are finalized by adding a 200 nm AlOx capping layer using a high vacuum electron-beam evaporator in order to make the samples more durable for the following steps. This increased the yield considerably. The samples are baked on a hotplate at 150 °C for 20 min before and after the AlOx evaporation in order to relieve internal stresses and reduce cracking.

To facilitate the fabrication of a heater and a thermometer, the PnC structures have a smooth platform for them on top and ramps for measurement leads. The top layer of spheres is left out except at the edges of the platform so that it is suspended in the middle [Fig. 1(d)]. The platform has a thickness of 1.6 μm, which is well within the 3D limit for the thermally dominant phonon modes. This geometry was chosen to reduce the direct ballistic flow of heat from the heater to the crystal, which would not create a signal at the thermometer; thus, the chosen geometry makes sure that the thermometer signal is measurable. The heater and thermometer are superconductor–insulator–normal metal–insulator–superconductor (SINIS) junction pairs fabricated opposing each other [Fig. 1(b)]. The junction pairs are fabricated onto the middle of the platform using a fabrication method developed by us for device fabrication on 3D topographies.[33] For these samples, aluminum was used as the superconductor and copper as the normal metal. The junction pairs can be used to measure the thermal conductance by biasing one of them to work as a thermometer and then heating the film with the other junction pair.[14]

III. SIMULATION METHODS

The sample geometry for the simulations was approximated as a 3D sphere array covered by a platform [partly suspended; see Fig. 1(d)] with a long rectangular heater on top of it. With the low temperatures (<1 K) used in the experiments, the flow of phonons is typically ballistic.[14,43] This means that the phonon emission is radiative and not diffusive. In the ballistic limit, the thermal conductance of the system can be calculated from the phonon emission power of the heater. The phonons emitted by the heater travel outward in all directions inside the suspended platform. In turn, the area of the platform that overlaps with the PnC can be considered to be a large area phonon source ("secondary heater") for the underlying PnC. In principle, these two parts of the sample give two contributions in series for the thermal conductance [Fig. 1(e)]. However, with the used dimensions of the samples, we calculated using Rayleigh–Lamb theory[44,45] that the thermal conductance of the platform is much higher than that of the PnC in the temperature range of the experiment (0.1–1 K) and does not limit the heat flow. The conductance of the platform is high, as it has essentially bulk behavior due to the softness of the material and the thickness of the platform (1.6 μm), with the 2D–3D crossover thickness[46] $d_C = \hbar c_t/(2k_BT)$ calculated to be as low as ~ 30 nm at 0.1 K for the IP-dip resist material.

With this information, we can calculate the phonon emission power of the platform flowing through the underlying 3D PnC structure. Only the outward propagating phonon modes with energies $\hbar\omega_j(\mathbf{k})$ carry the energy, so the phonon emission power is given by the 3D version of the expression given in Ref. 47,

$$P(T) = \frac{1}{8\pi^3}\sum_j \int_\gamma d\gamma \int_K d\mathbf{k}\hbar\omega_j(\mathbf{k})n(\omega_j, T) \times \frac{\partial\omega_j(\mathbf{k})}{\partial\mathbf{k}} \cdot \hat{\mathbf{n}}_\gamma \Theta\left(\frac{\partial\omega_j}{\partial\mathbf{k}} \cdot \hat{\mathbf{n}}_\gamma\right), \quad (1)$$

where γ represents a planar rectangular phonon source surface ("secondary heater") with area A, Θ is the Heaviside step function, $\hat{\mathbf{n}}_\gamma$ is the unit normal on the heater, and the $\mathbf{k}$-integral is taken over

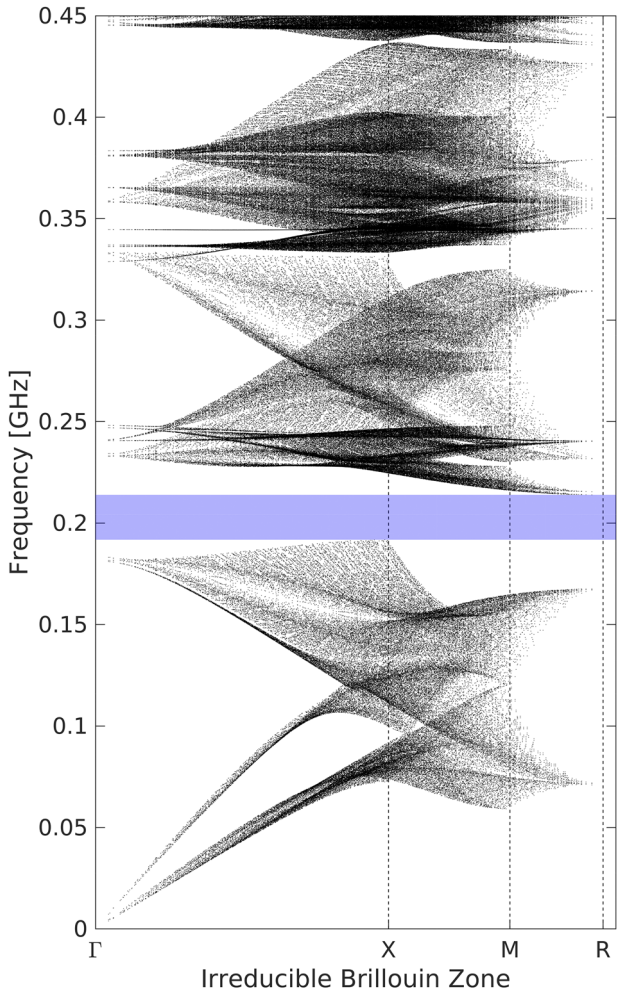

FIG. 2. The lowest spectral branches $\omega(\mathbf{k})$ given by the FEM simulations for the 3.1 μm PnC. The x-axis is the magnitude of the wavevector, with the distances to X, M, and R high symmetry points in the Brillouin zone marked by the vertical lines. A complete energy gap is marked in blue.

the first 3D Brillouin zone K. Here, $n(\omega, T)$ is the Bose–Einstein distribution describing the thermal occupation of the phonons and the term $\partial\omega_j/\partial\mathbf{k}$ describes the group velocity of the modes j. The only unknown in the expression is the set of dispersion relations $\omega_j = \omega_j(\mathbf{k})$, which can be calculated numerically using the finite element modeling (FEM) of continuous linear elasticity theory.[14] Here, we used the mesh shown in Fig. 1(f) to find these relations, where the diameter of the spheres and the contact area between them, being sensitive parameters[7,30] for $\omega_j(\mathbf{k})$, were determined by SEM imaging.

To calculate the band structure, the 3D irreducible Brillouin zones of the PnCs were first divided into small tetrahedrons, where the Gaussian quadrature points of the order 8 were identified. Phonon eigenfrequencies were solved up to 28 GHz (10 GHz) on the total of 13 672 (4096) quadrature points for the 3.1 μm (5 μm) geometries, respectively. An example of the lowest dispersion branches forming 3D point clouds for the 3.1 μm structure is shown in Fig. 2, as a function of the absolute value of the phonon wavevector. Group velocities (gradients) at the quadrature points were solved by finding 20 nearest neighbors for each point and then using the least squares algorithm to approximate the gradient of each branch. The material parameters used for the Ip-Dip resist were[48] $\rho = 1100$ kg/m^3, $E = 2.5$ GPa, and $\nu = 0.49$.

The final simulated curves in Fig. 3 for the phonon emission power were obtained from the FEM simulated data for the platform and the PnC using the real physical dimensions of the metallic heater and the horizontal contact area between the platform and the PnC or, in the case of the bulk reference sample, the vertical contact area between then platform and the bulk support (smaller). A series thermal resistance model was used [platform + PnC or bulk support, Fig. 1(e)], with the temperature at the interface calculated by setting the power flowing through the platform and the PnC (bulk) to be equal. For simplicity, zero bath temperature was assumed. This modeling confirmed our earlier assertion that for the PnC samples, the coherent ballistic thermal conductance is expected to be fully limited by the PnC itself, as the platform–PnC interface and SINIS heater temperatures were very close to equal.

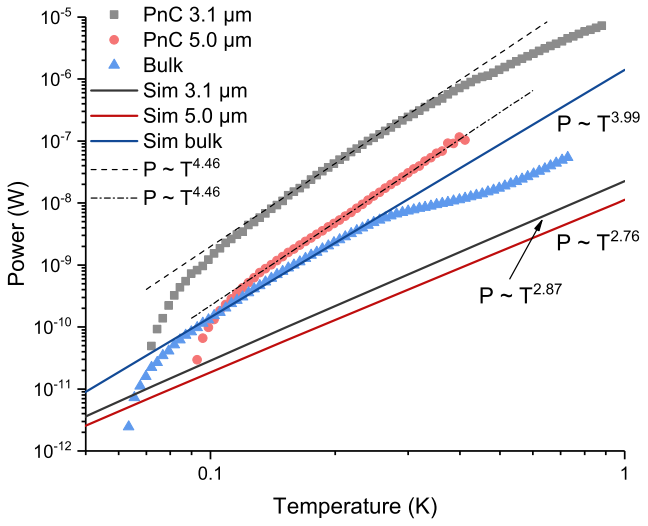

FIG. 3. The results of the thermal conductance measurements presented as the measured heating power of the SINIS heater (emitted phonon power) as a function of the measured temperature on the platform (colored symbols). The colored lines represent the results given by the FEM simulations for each sample, without any fitting parameters, assuming zero bath temperature for clarity. The dip at the high temperature end of the bulk data is likely caused by a non-ideality in the behavior of the thermometer junction.

IV. THERMAL CONDUCTANCE MEASUREMENT AND SIMULATION RESULTS

The thermal conductance of the fabricated structures was measured at sub-Kelvin temperatures utilizing a ^{3}He/^{4}He dilution refrigerator. These measurements were made for the two different simple cubic PnC structures with lattice constants 3.1 and 5.0 μm and also for a bulk sample with otherwise identical geometry, except that the PnC structure was substituted by a bulk resist. The measurements were done by first calibrating one of the SINIS junction pairs to work as a thermometer by measuring the response as a function of varying refrigerator (bath) temperatures. The thermal conductance experiment was then performed by Joule heating the second SINIS device and simultaneously measuring the temperature of the platform and the dissipated power using $P = IV$. The heating was done with a very slowly sweeping power to maintain quasi-equilibrium. The results of these measurements are shown in Fig. 3 together with the results from the FEM simulations.

From the measurements, it is clear that the PnC structures did alter the thermal conductance of the material very strongly, as there is a large difference to the bulk result and even between the two PnC structures. This also proves that the transport is mostly ballistic, as diffusive FEM calculations based on Fourier theory (not shown) showed identical results with all three geometries (limited by the platform). In addition, it is noticeable that the ballistic modeling explains the bulk results surprisingly well, without any fitting parameters. The observed temperature exponent of the bulk device is the expected $P \sim T^4$ value for 3D ballistic conduction.

However, the data for the PnC devices deviated very strongly from the modeling. As can be seen in Fig. 3, the coherent modeling predicts that the PnCs should decrease the thermal conductance, by about an order of magnitude, whereas the measurement shows a puzzling *increase*, up to an order of magnitude for the smaller period. In addition, the observed temperature exponent for the PnC devices, $P \sim T^{4.5}$, does not agree with the coherent modeling result, where a much weaker power law is expected. Very little is currently understood about this surprising enhancement. We speculate that it may have to do with thermal boundary resistance physics between a PnC and a solid structure, which has not been studied at all yet, or the effects of losses on the band structure,[49] which could be studied in more detail in the future.

V. CONCLUSIONS

We have shown that 3D direct-laser-write two-photon lithography is a viable method for the fabrication of 3D phononic crystal structures in the hypersonic frequency range, which allows applications in thermal sciences. The strength of the method is not only in the fact that it can be used to produce complex 3D

crystal structures; the same technique can also be used for the fabrication of measurement devices on the crystals. The thermal conductance experiments performed in the reported sub-Kelvin temperature range showed large up to an order of magnitude differences between the results obtained for phononic crystals and an otherwise identical bulk sample, demonstrating the potential for controlling thermal transport using 3D structures. However, the simplest FEM simulations based on the picture of fully coherent modification of the phononic band structure did not capture the essential features of the data. In particular, the used modeling predicts a reduction, whereas the experiments demonstrated a large enhancement of thermal conductance. This surprising enhancement is not understood yet.

ACKNOWLEDGMENTS

This study was supported by the Academy of Finland (Project Nos. 298667 and 341823). The authors would like to acknowledge the CSC-IT Center for Science, Finland, for computational resources. Technical support from Zhuoran Geng is acknowledged.

DATA AVAILABILITY

The data that support the findings of this study are available from the corresponding author upon reasonable request.

REFERENCES

[1]J. D. Joannopoulos, S. G. Johnson, J. N. Winn, and R. D. Meade, *Photonic Crystals: Molding the Flow of Light* (Princeton University Press, 2008).
[2]T. Vasileiadis, J. Varghese, V. Babacic, J. Gomis-Bresco, D. Navarro Urrios, and B. Graczykowski, "Progress and perspectives on phononic crystals," J. Appl. Phys. **129**, 160901 (2021).
[3]M. S. Kushwaha, P. Halevi, L. Dobrzynski, and B. Djafari-Rouhani, "Acoustic band structure of periodic elastic composites," Phys. Rev. Lett. **71**, 2022–2025 (1993).
[4]M. Sigalas and E. N. Economou, "Band structure of elastic waves in two dimensional systems," Solid State Commun. **86**, 141–143 (1993).
[5]Y. Pennec, J. O. Vasseur, B. Djafari-Rouhani, L. Dobrzyński, and P. A. Deymier, "Two-dimensional phononic crystals: Examples and applications," Surf. Sci. Rep. **65**, 229–291 (2010).
[6]M. Sledzinska, B. Graczykowski, J. Maire, E. Chavez-Angel, C. M. Sotomayor-Torres, and F. Alzina, "2D phononic crystals: Progress and prospects in hypersound and thermal transport engineering," Adv. Funct. Mater. **30**, 1904434 (2020).
[7]B. Graczykowski, N. Vogel, K. Bley, H.-J. Butt, and G. Fytas, "Multiband hypersound filtering in two-dimensional colloidal crystals: Adhesion, resonances, and periodicity," Nano Lett. **20**, 1883–1889 (2020).
[8]S. Yang, J. H. Page, Z. Liu, M. L. Cowan, C. T. Chan, and P. Sheng, "Focusing of sound in a 3D phononic crystal," Phys. Rev. Lett. **93**, 024301 (2004).
[9]S. Tol, F. L. Degertekin, and A. Erturk, "3D-printed phononic crystal lens for elastic wave focusing and energy harvesting," Addit. Manuf. **29**, 100780 (2019).
[10]J. A. Iglesias Martínez, J. Moughames, G. Ulliac, M. Kadic, and V. Laude, "Three-dimensional phononic crystal with ultra-wide bandgap at megahertz frequencies," Appl. Phys. Lett. **118**, 063507 (2021).
[11]T. Gorishnyy, C. K. Ullal, M. Maldovan, G. Fytas, and E. L. Thomas, "Hypersonic phononic crystals," Phys. Rev. Lett. **94**, 115501 (2005).
[12]W. Cheng, J. Wang, U. Jonas, G. Fytas, and N. Stefanou, "Observation and tuning of hypersonic bandgaps in colloidal crystals," Nat. Mater. **5**, 830–836 (2006).
[13]R. H. Olsson III and I. El-Kady, "Microfabricated phononic crystal devices and applications," Meas. Sci. Technol. **20**, 012002 (2008).
[14]N. Zen, T. A. Puurtinen, T. J. Isotalo, S. Chaudhuri, and I. J. Maasilta, "Engineering thermal conductance using a two-dimensional phononic crystal," Nat. Commun. **5**, 3435 (2014).
[15]M. Maldovan, "Phonon wave interference and thermal bandgap materials," Nat. Mater. **14**, 667–674 (2015).
[16]M. R. Wagner, B. Graczykowski, J. S. Reparaz, A. El Sachat, M. Sledzinska, F. Alzina, and C. M. Sotomayor Torres, "Two-dimensional phononic crystals: Disorder matters," Nano Lett. **16**, 5661 (2016).
[17]J. Maire, R. Anufriev, R. Yanagisawa, A. Ramiere, S. Volz, and M. Nomura, "Heat conduction tuning by wave nature of phonons," Sci. Adv. **3**, e1700027 (2017).
[18]Y. Tian, T. A. Puurtinen, Z. Geng, and I. J. Maasilta, "Minimizing coherent thermal conductance by controlling the periodicity of two-dimensional phononic crystals," Phys. Rev. Appl. **12**, 014008 (2019).
[19]F. A. Nutz and M. Retsch, "Tailor-made temperature-dependent thermal conductivity via interparticle constriction," Sci. Adv. **3**, eaao5238 (2017).
[20]W. Chen, D. Talreja, D. Eichfeld, P. Mahale, N. N. Nova, H. Y. Cheng, J. L. Russell, S.-Y. Yu, N. Poilvert, G. Mahan, S. E. Mohney, V. H. Crespi, T. E. Mallouk, J. V. Badding, B. Foley, V. Gopalan, and I. Dabo, "Achieving minimal heat conductivity by ballistic confinement in phononic metalattices," ACS Nano **14**, 4235–4243 (2020).
[21]C. Enss, *Cryogenic Particle Detection* (Springer, Berlin, 2005).
[22]A. N. Bolgar, D. D. Kirichenko, R. S. Shaikhaidarov, S. V. Sanduleanu, A. V. Semenov, A. Y. Dmitriev, and O. V. Astafiev, "A phononic crystal coupled to a transmission line via an artificial atom," Commun. Phys. **3**, 207 (2020).
[23]W. Kim, J. Zide, A. Gossard, D. Klenov, S. Stemmer, A. Shakouri, and A. Majumdar, "Thermal conductivity reduction and thermoelectric figure of merit increase by embedding nanoparticles in crystalline semiconductors," Phys. Rev. Lett. **96**, 045901 (2006).
[24]D. G. Cahill, P. V. Braun, G. Chen, D. R. Clarke, S. Fan, K. E. Goodson, P. Keblinski, W. P. King, G. D. Mahan, A. Majumdar, H. J. Maris, S. R. Phillpot, E. Pop, and L. Shi, "Nanoscale thermal transport. II. 2003–2012," Appl. Phys. Rev. **1**, 011305 (2014).
[25]B. S. Lee and J. S. Lee, "Thermal conductivity reduction in graphene with silicon impurity," Appl. Phys. A **121**, 1193–1202 (2015).
[26]J.-K. Yu, S. Mitrovic, D. Tham, J. Varghese, and J. R. Heath, "Reduction of thermal conductivity in phononic nanomesh structures," Nat. Nanotechnol. **5**, 718–721 (2010).
[27]P. E. Hopkins, C. M. Reinke, M. F. Su, R. H. Olsson III, E. A. Shaner, Z. C. Leseman, J. R. Serrano, L. M. Phinney, and I. El-Kady, "Reduction in the thermal conductivity of single crystalline silicon by phononic crystal patterning," Nano Lett. **11**, 107–112 (2011).
[28]R. Anufriev, J. Maire, and M. Nomura, "Reduction of thermal conductivity by surface scattering of phonons in periodic silicon nanostructures," Phys. Rev. B **93**, 045411 (2016).
[29]P. Jiang, J. F. Bertone, K. S. Hwang, and V. L. Colvin, "Single-crystal colloidal multilayers of controlled thickness," Chem. Mater. **11**, 2132 (1999).
[30]T. J. Isotalo, Y. L. Tian, and I. J. Maasilta, "Fabrication and modelling of three-dimensional sub-kelvin phononic crystals," J. Phys.: Conf. Ser. **400**, 052007 (2012).
[31]T. J. Isotalo, Y.-L. Tian, M. P. Konttinen, and I. J. Maasilta, "Statistical characterization of self-assembled colloidal crystals by single-step vertical deposition," Colloids Surf., A **443**, 164–170 (2014).
[32]Y. Tian, T. J. Isotalo, M. P. Konttinen, J. Li, S. Heiskanen, Z. Geng, and I. J. Maasilta, "Integrating metallic wiring with three-dimensional polystyrene colloidal crystals using electron-beam lithography and three-dimensional laser lithography," J. Phys. D: Appl. Phys. **50**, 055302 (2017).
[33]S. Heiskanen and I. J. Maasilta, "Superconducting tunnel junction fabrication on three-dimensional topography based on direct laser writing," Appl. Phys. Lett. **117**, 232601 (2020).
[34]H.-B. Sun, S. Matsuo, and H. Misawa, "Three-dimensional photonic crystal structures achieved with two-photon-absorption photopolymerization of resin," Appl. Phys. Lett. **74**, 786–788 (1999).

[35]M. Deubel, G. von Freymann, M. Wegener, S. Pereira, K. Busch, and C. M. Soukoulis, "Direct laser writing of three-dimensional photonic-crystal templates for telecommunications," Nat. Mater. **3**, 444–447 (2004).
[36]S. Kawata, H.-B. Sun, T. Tanaka, and K. Takada, "Finer features for functional microdevices," Nature **412**, 697–698 (2001).
[37]L. D'Alessandro, E. Belloni, R. Ardito, A. Corigliano, and F. Braghin, "Modeling and experimental verification of an ultra-wide bandgap in 3D phononic crystal," Appl. Phys. Lett. **109**, 221907 (2016).
[38]F. Warmuth, M. Wormser, and C. Körner, "Single phase 3D phononic band gap material," Sci. Rep. **7**, 3843 (2017).
[39]F. Lucklum and M. J. Vellekoop, "Bandgap engineering of three-dimensional phononic crystals in a simple cubic lattice," Appl. Phys. Lett. **113**, 201902 (2018).
[40]O. McGee, H. Jiang, F. Qian, Z. Jia, L. Wang, H. Meng, D. Chronopoulos, Y. Chen, and L. Zuo, "3D printed architected hollow sphere foams with low-frequency phononic band gaps," Addit. Manuf. **30**, 100842 (2019).
[41]N. Aravantinos-Zafiris, F. Lucklum, and M. M. Sigalas, "Complete phononic band gaps in the 3D Yablonovite structure with spheres," Ultrasonics **110**, 106265 (2021).
[42]J. S. Oakdale, J. Ye, W. L. Smith, and J. Biener, "Post-print UV curing method for improving the mechanical properties of prototypes derived from two-photon lithography," Opt. Express **24**, 27077–27086 (2016).
[43]I. J. Maasilta, T. A. Puurtinen, Y. Tian, and Z. Geng, "Phononic thermal conduction engineering for bolometers: From phononic crystals to radial Casimir limit," J. Low Temp. Phys. **184**, 211 (2016).
[44]K. F. Graff, *Wave Motion in Elastic Solids* (Oxford University Press, 1975).
[45]T. Kühn, D. V. Anghel, J. P. Pekola, M. Manninen, and Y. M. Galperin, "Heat transport in ultrathin dielectric membranes and bridges," Phys. Rev. B **70**, 125425 (2004).
[46]T. Kühn and I. J. Maasilta, "Maximizing phonon thermal conductance for ballistic membranes," J. Phys.: Conf. Ser. **92**, 012082 (2007).
[47]T. A. Puurtinen and I. J. Maasilta, "Low-temperature coherent thermal conduction in thin phononic crystal membranes," Crystals **6**, 72 (2016).
[48]E. D. Lemma, F. Rizzi, T. Dattoma, B. Spagnolo, L. Sileo, A. Qualtieri, M. De Vittorio, and F. Pisanello, "Mechanical properties tunability of three-dimensional polymeric structures in two-photon lithography," IEEE Trans. Nanotechnol. **16**, 23–31 (2016).
[49]R. P. Moiseyenko and V. Laude, "Material loss influence on the complex band structure and group velocity in phononic crystals," Phys. Rev. B **83**, 064301 (2011).